Available online at www.sciencedirect.com

SCIENCE @ DIRECT®

Journal of the European Ceramic Society 24 (2004) 2707–2715

www.elsevier.com/locate/jeurceramsoc

Changes in microstructure and physico-chemical properties of hydroxyapatite–silk fibroin nanocomposite with varying silk fibroin content

Li Wang, Rei Nemoto, Mamoru Senna*

Department of Applied Chemistry, Faculty of Science and Technology, Keio University, 3-14-1 Hiyoshi, Yokohama 223-8522, Japan

Received 9 April 2003; received in revised form 5 September 2003; accepted 13 September 2003

Abstract

Hydroxyapatite (HAp)–silk fibroin (SF) nanocomposites with various HAp/SF weight ratios were synthesized by a co-precipitation method. We examined the effects of SF content on the microstructure and physico-chemical properties of the composites. Growth of HAp crystallites in both directions, i.e. along the *c*- and *a*-axes, was suppressed by the introduction of SF. With SF content increased up to 40 wt.%, the particle size distribution became narrower and the Vickers microhardness of the composites increased by a factor of 4. The composites exhibited the porous microstructure with open porosity around 62–74%. About 70% of the interconnective pores were between 40 and 115 μm in diameter. Among all the as-prepared samples, the composite containing 30 wt.% of SF showed the most homogeneous particle form and a well dispersed state of HAp crystallites together with a highly developed three-dimensional network.

Keywords: Composites; Crystallographic properties; Hydroxyapatite; Porosity; Silk fibroin content; Vickers microhardness

1. Introduction

It is well known that in many natural materials such as bone, cartilage, shells, and skin, inorganic minerals coexist with organic molecules in a well-organized manner.[1] Natural bone is a composite material comprising about 70 wt.% of a mineral phase, primarily hydroxyapatite (HAp), and 30 wt.% of an organic matrix.[2–4] It is this distinctive harmony between inorganic and organic phases that imparts homogeneous porous microstructure as well as sufficient mechanical toughness and flexibility to natural bone, so that it can serve as a scaffold for the vertebrate animal's body.

Over the past decades, growing interest has been focused on the development of inorganic–organic hybrid biomaterials in order to mimic natural materials' composition and structure. A minority component of organic macromolecules in ceramics such as proteins or polymers are usually used to control nucleation and growth of inorganic crystals, and thus to improve microstructure and physical properties. This related methodology has a great potential for the design and engineering of novel biomaterials with special functionalities.[1] It is also adopted in the fabrication of HAp-based composites, since the involvement of proteins or polymers such as collagen,[2–5] silk fibroin (SF),[6,7] gelatin,[8,9] chitosan[10–12] or chondroitin sulfate,[13–15] even in small amounts, can remarkably improve HAp's resistance to fracture and impede the migration tendency of HAp particles from the implanted sites.

SF is a linear polypeptide comprising 17 amino acids, mainly nonpolar ones such as alanine and glycine. SF with β-sheet structure has been extensively utilized in wound dressing areas owing to its appreciable bioactivity, high mechanical toughness and good oxygen permeability.[16–18]

Recently, a variety of porous HAp ceramics have been developed for bone replacement and remodeling.[19–24] Porous implants allow cells from the surrounding soft tissues to migrate into the pores so as to accelerate the proliferation and differentiation of cells. Body fluid and blood can infiltrate into the pores

---

* Corresponding author. Tel.: +81-45-566-1569; fax: +81-45-564-0950.

E-mail address: senna@applc.keio.ac.jp (M. Senna).

0955-2219/$ - see front matter © 2003 Elsevier Ltd. All rights reserved.
doi:10.1016/j.jeurceramsoc.2003.09.006

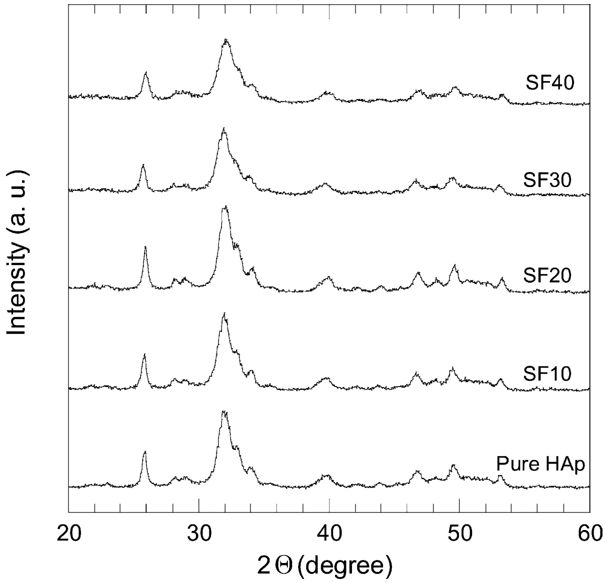

Fig. 1. X-ray diffraction profiles of pure HAp and HAp–SF composites with various SF content.

Table 1
Crystallographic parameters of HAp crystallites

Sample	SF content (wt.%)	L_c[a] (nm)	ε_c[a] (%)	L_a[a] (nm)	ε_a[a] (%)	L_c/L_a	S[b]
Pure HAp	0	21.4	0.56	8.0	0.87	2.66	1.34
SF10	10	19.9	0.43	8.0	0.79	2.48	1.31
SF20	20	19.5	0.43	8.1	0.66	2.42	1.40
SF30	30	17.7	0.50	7.2	0.87	2.46	1.31
SF40	40	15.9	0.71	6.4	0.90	2.49	1.39

[a] L represents the crystallite size and ε represents the lattice microstrain. Subscripts c and a represent along c-axis and along a-axis, respectively.

[b] S is a numerical criterion to indicate agreement between the observed and the calculated intensity distributions.

to supply nutrient and mineral ions for further bone ingrowth. Hence, new bone formation and attachment between implant and host living tissues can be promoted. It has been accepted that a minimum pore size of about 100–150 μm is required for bone ingrowth. Therefore, much attention has been paid to the development of porous HAp ceramics with particular pore size and pore volume.

In our previous work, we synthesized HAp–SF nanocomposite containing 9 wt.% of SF via a wet-mechanochemical route.[25] It has been found that there is an enhanced three-dimensional porous microstructure in the composite in comparison with the synthetic pure HAp without SF; that is formed via the crosslinkage between HAp clusters and SF fibrils. In the present study, HAp–SF composites with various amounts of SF were prepared by a co-precipitation method attempting to obtain well-dispersed HAp nanoparticles in a SF matrix. Our efforts were focused on the effects of SF content on the microstructure and hardness of the composites along with crystallographic properties of HAp.

2. Experimental

2.1. Preparation of HAp–SF composites

The starting materials were $Ca(OH)_2$ (Wako Pure Chemical Inc.), H_3PO_4 (Taisei Pure Chemical Inc.) of analytical grade, and SF (K-50, donated by Idemitsu Technofine Co., Ltd.). SF K-50 is a hard protein with β-sheet structure extracted from silk cocoon and contains 70 wt.% of fibroin and 30 wt.% of sericin.[25] SF we employed is of super fine powder with an apparent density of 0.25–0.45 g/cm^3 and has homogeneous globular morphology and good dispersivity in water. The SF powder shows a single-modal particle size distribution bracketing the range of 0.9–15 μm with an average size of 5–6 μm.

Fifty-five milliliter 1.57 M H_3PO_4 solution was added dropwise into 155 g 6 wt.% of $Ca(OH)_2$ suspension containing various amounts of SF powder. The molar ratio of Ca/P in the starting mixture was set as 1.67, equal to that of stoichiometric HAp. The weight ratios of HAp/SF in the final products were regulated to be 90/10, 80/20, 70/30 and 60/40. The samples obtained are hereafter designated as SF10, SF20, SF30 and SF40, respectively. The mixture was stirred vigorously at room temperature for 3 h, followed by centrifugation and water-washing alternately for three cycles to harvest the precipitates. The precipitates were vacuum-dried at 50 °C for 24 h and subsequently ground into fine powders using an agate mortar. Meanwhile, pure HAp without SF was prepared as a control sample by the same process. For hardness measurement, the powder samples were compressed into cylindrical tablets with a diameter of 11.3 mm and a height of 3.6 mm under a load of 98 MPa for 3 min.

2.2. Characterization of the materials

The as-prepared powders were examined using X-ray diffractometer (XRD) (RINT 2200, Rigaku Co., Tokyo) with Cu$K\alpha$ radiation. The X-ray diffraction data were collected in 2θ range of 10–120° with a step size of 0.05° and a counting time of 10 s. Crystallographic parameters of HAp were determined based on the refinement of these XRD data by Rietveld analysis, a computer program (called as RIETAN 2000) developed by Izumi and Rigaku Limited Company.[26] An enhanced laser diffraction granulometer (Beckman Coulter, LS230) was used to analyze particle size distribution. Microstructural observations were performed on a transmission electron microscope (TEM) (Philips,

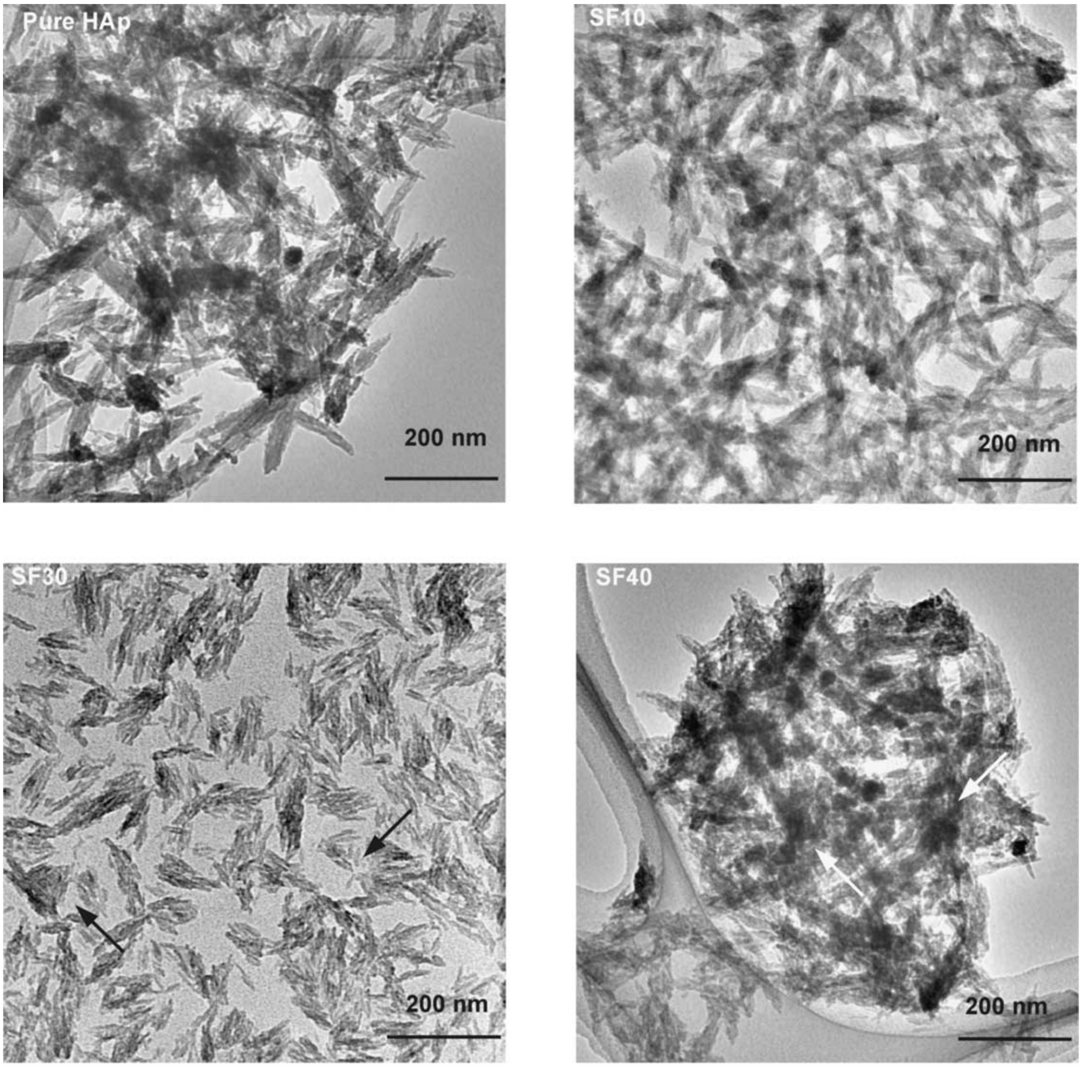

Fig. 2. TEM micrographs of pure HAp and HAp–SF composites. Aggregates consisting of needle-like crystallites represent the crystalline phase of HAp, as indicated by the white arrows. Silk fibroin and the amorphous phase of HAp are indicated by the black arrows.

Table 2
Results of particle size distribution

Sample	Average particle size (μm)	Median particle size (μm)	Bottom particle size (μm)	Top particle size (μm)	FWHM[a] (μm)
Pure HAp	9.5	7.9	1.3	52.6	16.5
SF10	9.5	7.7	1.0	47.9	15.0
SF20	9.0	7.6	1.1	33.0	15.0
SF30	8.5	7.3	1.4	27.4	13.0
SF40	8.0	7.3	1.0	25.0	12.0

[a] FWHM is full width at half maximum of particle size distribution curve.

TECNAI F20) and a scanning electron microscope (SEM, Hitachi, S-4700), respectively. Pore size distribution was evaluated by mercury porosimetry (CE Instrument, PASCAL140 and PASCAL440). Microhardness of the compressed tablets was measured by means of a Vickers microhardness tester (AKASHI MVK-FII). A pyramidal diamond indenter was applied to the tablet surface under a load of 0.098 N for 15 s. Diagonal length of the indentation was measured through a micometric eyepiece with an objective lens of 40×. The tests were repeated five times for each sample.

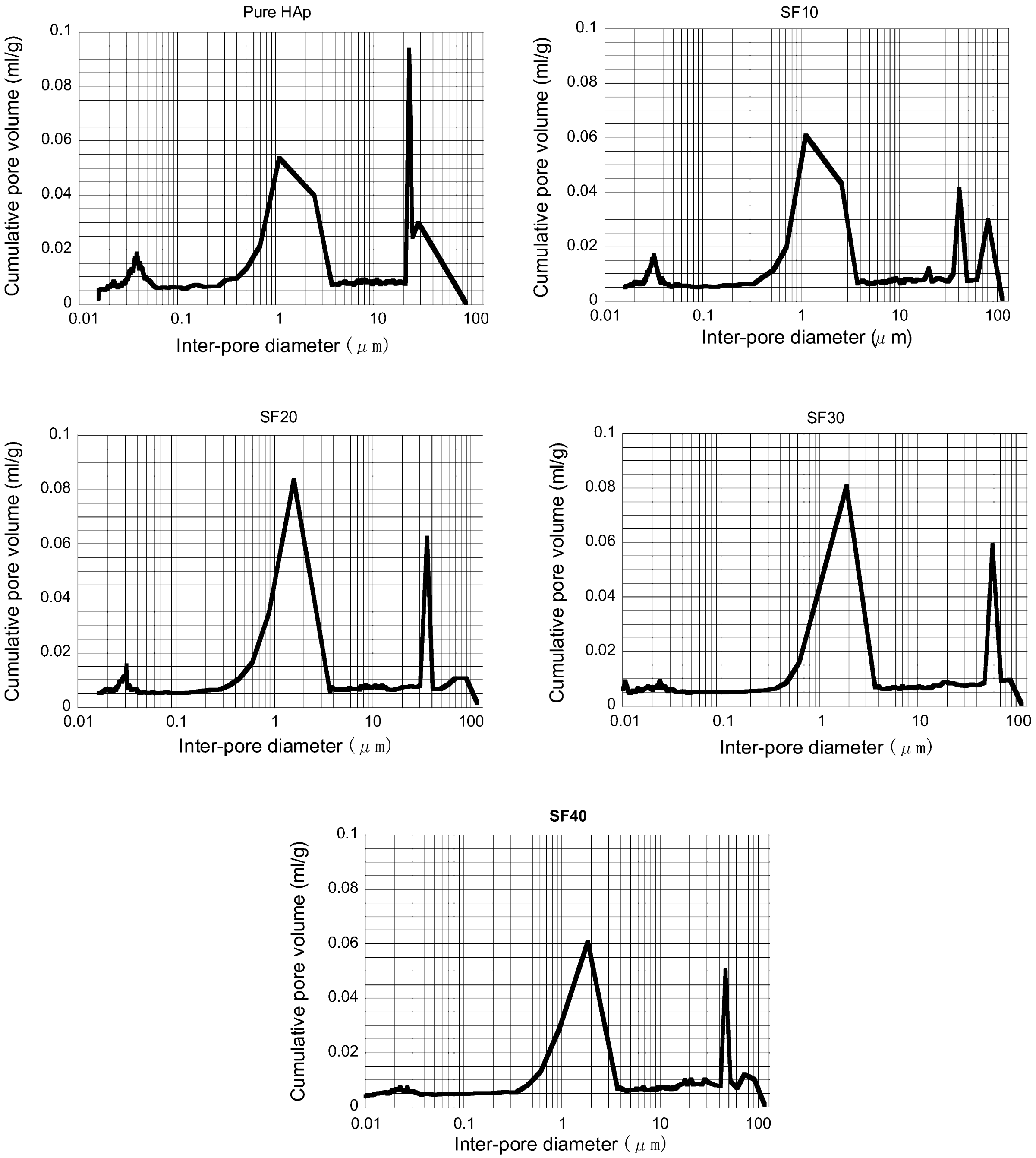

Fig. 3. Representative pore size distributions of pure HAp and HAp–SF composites.

Table 3
Total open pore volume and pore size distribution

Sample	Total cumulative open pore volume (cm^3/g)	Pore contents at different pore size dimensions (vol%)		
		<10 μm	10–40 μm	40–115 μm
Pure HAp[a]	1.24	12		
SF10	1.15	10	22	68
SF20	1.11	12	18	70
SF30	0.94	12	16	72
SF40	0.88	12	21	67

[a] For pure HAp, the volume fraction of pore contents between 10–87 μm is 88%. Its pore distribution between 28–87 μm is not continuous and its largest pore diameter is 87 μm.

3. Results and discussion

3.1. Crystallographic features and morphology of HAp

X-ray diffraction patterns in Fig. 1 reveal that all the peaks are well defined and assigned only to crystalline HAp, since no secondary phase can be detected even in the samples containing relatively large amounts of SF. Crystallographic parameters of HAp crystallites derived from Rietveld refinement are listed in Table 1. A common Rietveld analysis requires that the goodness of fit indicator (*S*) is less than 2.0 to ensure the calculated results are reliable.[26] The *S* values between 1.3 and 1.4 for all the samples are low enough to meet the requirement very well. With SF content increasing, the crystallite sizes are reduced both along *c*-axis (L_c) and along *a*-axis (L_a). There is no significant variation found in the aspect ratio of L_c/L_a of HAp crystallites with SF content. The lattice microstrain remains below 1%. These findings tell us the addition of SF suppresses the crystallite growth of HAp without increasing lattice microstrain.

As seen in Fig. 2, needle-like HAp nanocrystals aggregate into clusters in pure HAp and HAp–SF composites. We also observe the reduced agglomeration by increasing SF content to 30 wt.% and a well dispersed state of HAp crystallites in SF30. However, the aggregation becomes much more severe again as SF content reaches 40 wt.%. This means the extent of aggregation of HAp crystals is not decreased but intensified by adding more than 30 wt.% of SF. Due to the introduction of SF fine powder in the appropriate amount of 30 wt.%, a very homogeneous mixture for the original materials as well as a lot of small foams was produced in the synthesis process. This may create a favorable microenvironment for HAp particles to remain their sizes small enough with a uniform distribution.

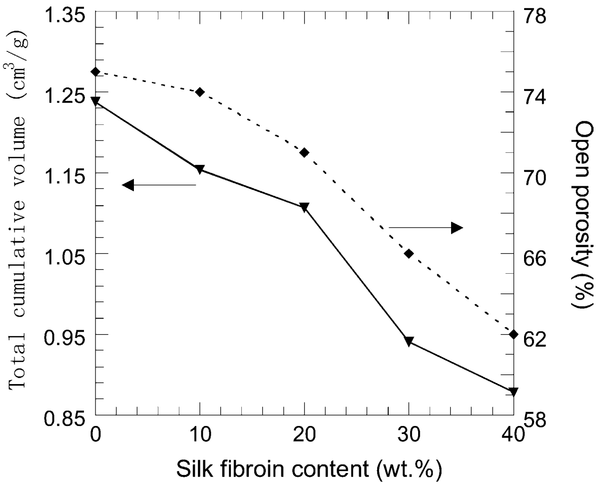

Fig. 4. Variations in total cumulative pore volume and open porosity as a function of SF content for pure HAp and HAp–SF composites.

All the samples show monomodal particle size distributions. As shown in Table 2, the size distribution tends to be narrower and the average particle size decreases from 9.5 to 8.0 μm when the SF content increased to 40 wt.%. It can be inferred that SF serves as a dispersant to lessen the aggregation of particles. However, the dispersivity of SF in excessive amounts is actually limited as evidenced by the similar distributions between SF30 and SF40.

3.2. Pore size distribution

As for the pore size distribution (Fig. 3), a typical bimodal style is found in SF30 and SF40, while more than two peaks are observed in the samples of pure HAp, SF10 and SF20. About 67–72% of the interpores range from 40 to 115 μm in diameter. Bulk density (D_b = sample weight/sample volume) and apparent density [$D_{ap} = 1/(1/D_b - V_{cumu})$, where V_{cumu} is total cumulative pore volume per gram of sample expressed by cm^3/g] are obtained from mercury porosimetry. Then we calculated total porosity ($P_{total} = 1 - D_b/D_{st}$, $D_{st} = 3.16$ g/cm^3, the theoretical density of HAp), open porosity ($P_{open} = 1 - D_b/D_{ap}$) and closed porosity ($P_{closed} = P_{total} - P_{open}$).[20,22] The porous properties derived from mercury porosimetry are summarized in Tables 3 and 4. The variations in V_{cumu} or P_{open} as a function of SF content are described in Fig. 4. From SF10 to SF40, V_{cumu} and P_{open} decrease by 23 and 16%, respectively. It illustrates that the texture becomes slightly denser with SF content increasing, which is most likely attributed to the intimate crosslinkage between HAp clusters and SF fibrils.

Table 4
Different densities and porosities

Sample	Bulk density (g/cm^3)	Apparent density (g/cm^3)	Total porosity (%)	Open porosity (%)	Open/total porosity (%)
Pure HAp	0.59	2.18	81	75	93
SF10	0.64	2.45	79	74	93
SF20	0.64	2.19	80	71	89
SF30	0.70	2.04	78	66	84
SF40	0.70	1.84	78	62	80

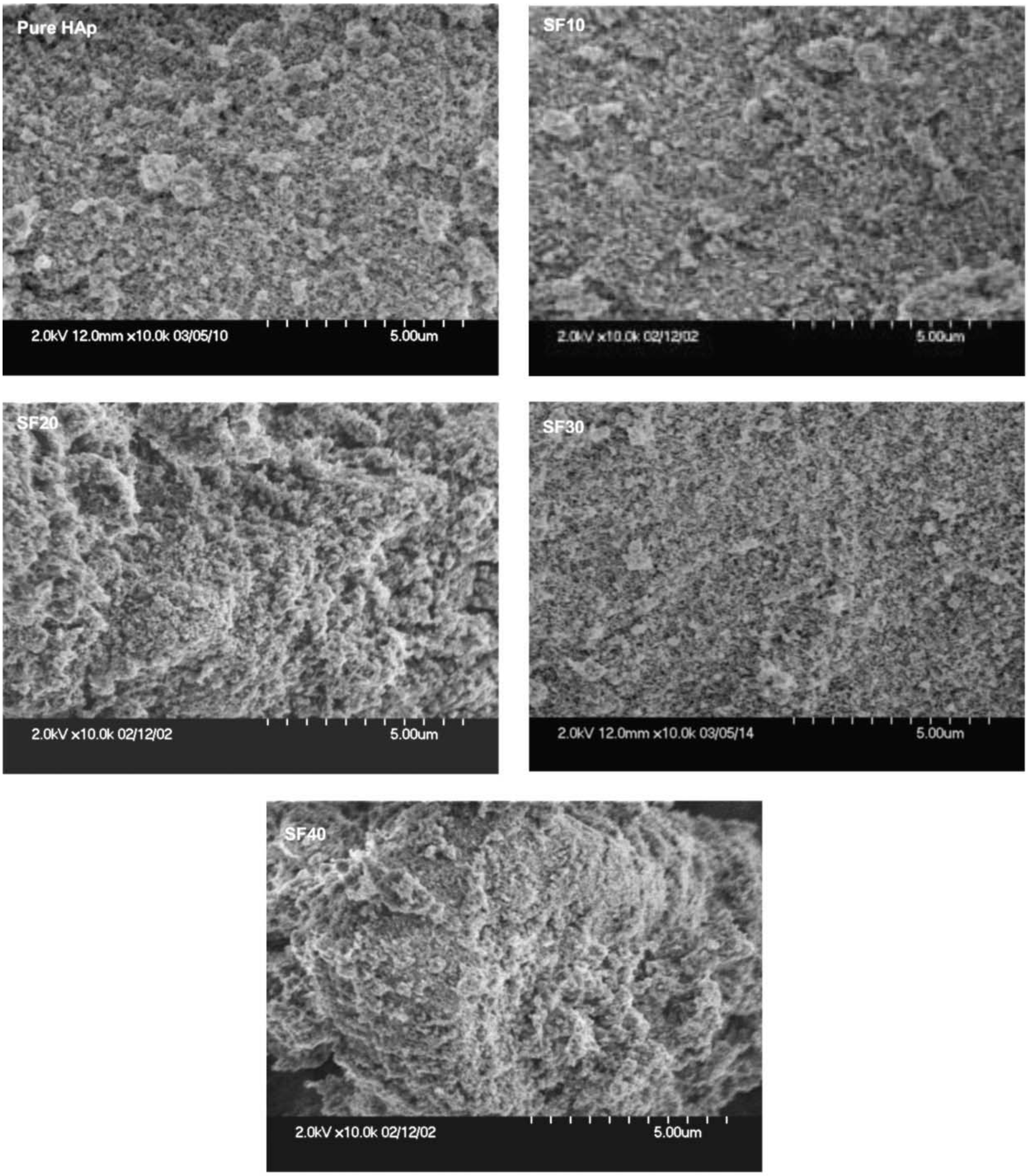

Fig. 5. SEM images of pure HAp and HAp–SF composites.

The open porosity accounts for above 80% of the total porosity for all the samples.

3.3. Microstructure

SEM micrographs in Fig. 5 display the microstructure of pure HAp and the composites. With SF content increased from 10 to 30 wt.%, surface roughness of the composites decreases and the crosslinkage between HAp clusters and SF fibrils is reinforced. When SF content is increased to 40 wt.%, the surface becomes irregular again. The pore size distribution tends to be more uniform with SF content increasing and the most uniform one appears in SF30, corresponding to the narrower particle size distribution with SF content increasing. In SF30, an enhanced three-dimensional network extending throughout the composites is formed via the intimate crosslinkage between HAp clusters and SF fibrils. A possible explanation for these findings is proposed in the following, as schematically illustrated in Fig. 6. Here we suppose SF fibrils act as organic matrix to provide active sites available for the nucleation and growth of HAp crystallites. In pure synthetic HAp or the composites with lower SF content than 30 wt.%, the active sites offered by the organic matrix are insufficient. HAp nanocrystallites randomly aggregate into clusters and the clusters loosely bond together [Fig. 6(a)]. Therefore, loose microstructure with irregular pore size distribution is observed in the samples of pure HAp, SF10 and SF20. In the composite containing 30 wt.% of SF, the organic matrix in the suitable amount may provide larger number of active sites, which can promote the self-assembly of HAp crystallites on SF fibrils. Hence, the HAp clusters are crosslinked with SF fibrils in a more intimate manner, so that a well developed three-dimensional network can be formed throughout the composites as depicted in Fig. 6(b). However, excessive amounts of SF may induce severe entanglement among SF fibrils to alter the microstructure. This will be discussed below in view of the relationship between Vickers microhardness and porosity.

3.4. Microhardness

The diagonal length of the micro Vickers indentations, between 20 and 44 µm, is much larger than the average aggregate size, i.e. 8.0–9.5 µm. On this basis, we may reasonably assume that the microhardness reflects the strength of the connections among aggregates, rather than within an aggregate.

As shown in Fig. 7, the Vickers microhardness increases by four times with SF content increased to 40 wt.%. On the contrary, open porosity decreases with SF content increasing. It is commonly accepted that the hardness of the porous materials decreases with the porosity increasing.[22,24] Synthetic porous HAp-based materials with larger pore size and higher porosity are usually weak in mechanical toughness, which limits their biomedical applications as load-bearing implants.[22,24] The correlation between the Vickers microhardness and the open porosity shown in Fig. 8 is expressed by an empirical equation:

$$\mathrm{HV} = 1791 - 80.42P_{\mathrm{open}} + 1.229P_{\mathrm{open}}^2 - 0.006313P_{\mathrm{open}}^3 \tag{1}$$

where HV is the Vickers microhardness, P_{open} is the open porosity (%). It is recognized that the experimental data of SF40 apparently deviate from the regression curve. This deviation strongly suggests that the nature of the inter-aggregate interaction in SF40 is

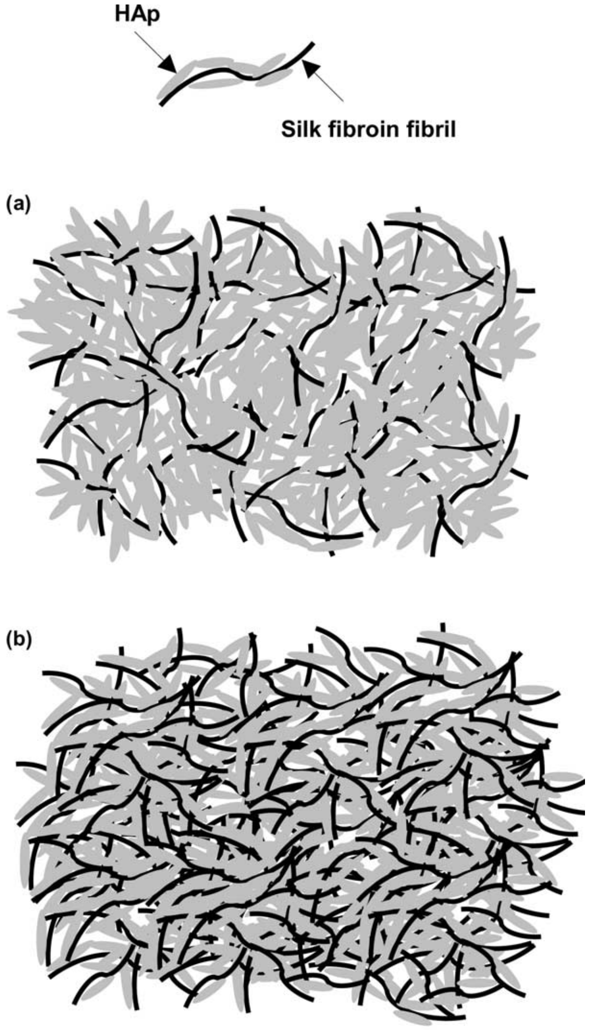

Fig. 6. Schematic structure models: (a) the composite with low SF content of 10 wt.%, (b) the proposed three-dimensional network in the composite containing 30 wt.% of SF.

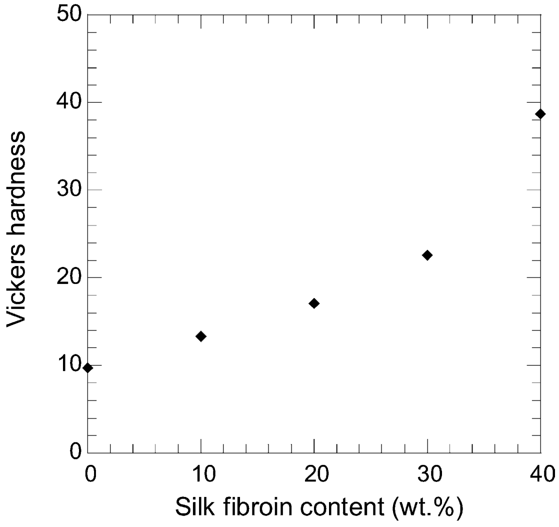

Fig. 7. Variations in the Vickers microhardness of the compressed specimens versus SF content.

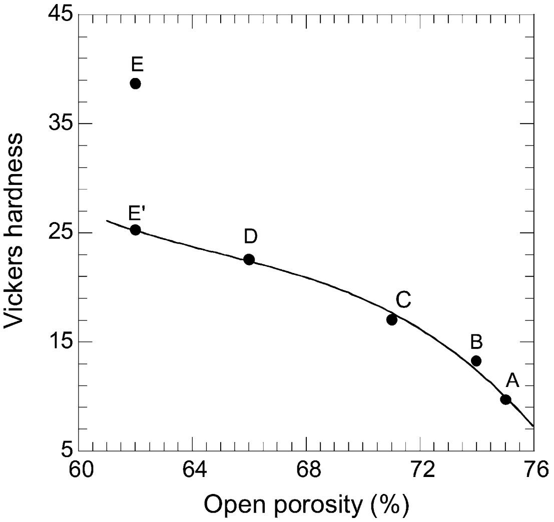

Fig. 8. Relationship between the Vickers microhardness and open porosity: solid circles A, B, C, D and E for the experimental data of pure HAp, SF10, SF20, SF30 and SF40, respectively, solid line for the empirical regression curve, solid circle E′ for the theoretical hardness of SF40 obtained from the regression curve.

qualitatively different from that in the other samples. The introduction of SF in excessive amounts inevitably increases the number density of inter aggregate contacts. This may lead to more severe entanglement among SF fibrils on the surface of the aggregates. Accordingly, the mechanical interaction among HAp aggregates could be significantly reinforced by the entanglement at inter aggregate boundary. This explains why we observe a sharp increase in the microhardness from SF30 to SF40. More explicit evidences are yet to be explored with this regard.

From the microstructural and physico-chemical viewpoints, we may conclude that the HAp–SF composite with 30 wt.% of SF, having similar composition to that of natural bone, would be taken as the first option to do further essential investigations on optimization of porous properties, improvement in mechanical strength and biological tests in animals toward the practical clinical application in the near future.

4. Conclusions

HAp–SF nanocomposites with about 70% of open porosity and most of the interpores ranging from 40 to 115 μm in diameter were obtained by a co-precipitation method. The protein SF plays a templating role to provide active sites for the nucleation and growth of HAp crystallites, so that a well-dispersed state of HAp crystals can be achieved, particularly in the composites containing 30 wt.% of SF. The down sizing of HAp crystallites with SF content increasing is most likely associated with the promoted nucleation with limited growth in a microenvironment created by SF matrix. In the composites, the needle-like HAp nanocrystallites aggregate into clusters and the clusters are crosslinked with SF fibrils to form a three-dimensional porous network. Among all the products, the composite comprising 70 wt.% HAp and 30 wt.% SF, exhibits the most uniform pore size distribution and the most regular particle surface together with an enhanced three-dimensional network. Microhardness of the as-prepared materials is increased by the introduction of SF matrix. There is a sharp increase in microhardness as SF content increased from 30 to 40 wt.%, which is interpreted by the severe entanglement among SF fibrils at the boundary of inter HAp aggregates in the composites with excessive amounts of SF.

Acknowledgements

This work was partially supported by Keio Life Conjugate Chemistry (LCC) Program of COE Research Project sponsored by Japanese Ministry of Education, Science Culture, and Sports. The authors would like to thank Idemitsu Technofine Co., Ltd. for its donation of silk fibroin powder, Mr. T. Murase and Ms. S Shimanuki for their technical assistance in mercury porosimetry measurement and TEM observations, respectively. One of the authors, L. Wang also gratefully acknowledges the financial support of Yoshida Scholarship Foundation during her doctoral fellowship in Japan.

References

1. Stupp, S. I. and Braun, P. V., Molecular manipulation of microstructures: biomaterials, ceramics, and semiconductors. *Science*, 1997, **277**, 1242–1248.
2. TenHuisen, K. S., Martin, R. I., Klimkiewicz, M. and Brown, P. W., Formation and properties of a synthetic bone composite: hydroxyapatite-collagen. *J. Biomed. Mater. Res.*, 1995, **29**, 803–810.
3. Kikuchi, M., Itoh, S., Ichinose, S., Shinomiya, K. and Tanaka, J., Self-organization mechanism in a bone-like hydroxyapatite/collagen nanocomposite synthesized in vitro and its biological reaction in vivo. *Biomaterials*, 2001, **22**, 1705–1711.
4. Du, C., Cui, F. Z., Zhang, W., Feng, Q. L., Zhu, X. D. and Groot, K.De., Formation of calcium phosphate/collagen composites through mineralization of collagen matrix. *J. Biomed. Mater. Res.*, 2000, **50**, 518–527.
5. Chang, M. C., Ikoma, T., Kikuchi, M. and Tanaka, J., Preparation of a porous hydroxyapatite/collagen nanocomposite using glutaraldehyde as a crosslinkage agent. *J. Mater. Sci. Lett.*, 2001, **20**, 1199–1201.
6. Furuzono, T., Taguchi, T., Kishida, A., Akashi, M. and Tamada, Y., Preparation and characterization of apatite deposited on silk fabric using an alternate soaking process. *J. Biomed. Mater. Res.*, 2000, **50**, 344–352.

7. Nemoto, R., Nakamura, S., Isobe, T. and Senna, M., Direct synthesis of hydroxyapatite-silk fibroin nano-composite sol via a mechanochemical route. *J. Sol-Gel Sci. Technol.*, 2001, **21**, 7–12.
8. Yin, Y. J., Zhao, F., Song, X. F., Yao, K. D., Lu, W. W. and Leong, J. C., Preparation and characterization of hydroxyapatite/chitosan-gelatin network composite. *J. Appl. Polym. Sci.*, 2000, **77**, 2929–2938.
9. Bigi, A., Boanini, E., Panzavolta, S., Roveri, N. and Rubin, K., Bonelike apatite growth on hydroxyapatite-gelatin sponges from simulated body fluid. *J. Biomed. Mater. Res.*, 2002, **59**, 709–714.
10. Ito, M., Hidaka, Y., Nakajima, M., Yagasaki, H. and Kafrawy, A. H., Effect of hydroxyapatite content on physical properties and connective tissue reactions to a chitosan-hydroxyapatite composite membrane. *J. Biomed. Mater. Res.*, 1999, **45**, 204–208.
11. Yamaguchi, I., Tokuchi, K., Fukuzaki, H., Koyama, Y., Takakuda, K., Monma, H. and Tanaka, J., Preparation and microstructure analysis of chitosan/hydroxyapatite nanocomposites. *J. Biomed. Mater. Res.*, 2001, **55**, 20–27.
12. Sunny, M. C., Ramesh, P. and Varma, H. K., Microstructured microspheres of hydroxyapatite bioceramic. *J. Mater. Sci.: Mater. Med.*, 2002, **13**, 623–632.
13. Murata, N., Osaka, A., Rhee, S. H., Miyazaki, K., Sakura, Y., Ikoma, T. and Tanaka, J., The preparation of hydroxyapatite and chondroitin sulfate composites. *Bioceramics*, 1999, **12**, 429–432.
14. Rhee, S. H. and Tanaka, J., Effect of chondroitin sulfate on the crystal growth of hydroxyapatite. *J. Am. Ceram. Soc.*, 2000, **83**, 2100–2102.
15. Rhee, S. H. and Tanaka, J., Self-assembly phenomenon of hydroxyapatite nanocrystals on chondroitin sulfate. *J. Mater. Sci.: Mater. Med.*, 2002, **13**, 597–600.
16. Park, S. J., Lee, K. Y., Ha, W. S. and Park, S. Y., Structural changes and their effect on mechanical properties of silk fibroin/chitosan blends. *J. Appl. Polym. Sci.*, 1999, **74**, 2571–2575.
17. Kweon, H., Ha, H. C., Um, I. C. and Park, Y. H., Physical properties of silk fibroin/chitosan blend films. *J. Appl. Polym. Sci.*, 2001, **80**, 928–934.
18. Freddi, G., Monti, P., Nagura, M., Gotoh, Y. and Tsukada, M., Structure and molecular conformation of tussah silk fibroin films: effect of heat treatment. *J. Polym. Sci. B: Polym. Phys.*, 1997, **35**, 841–847.
19. Sepulveda, P., Binner, J. G. P., Rogero, S. O., Higa, O. Z. and Bressiani, J. C., Production of porous hysroxyapatite by the gel-casting of foams and cytotoxic evaluation. *J. Biomed. Mater. Res.*, 2000, **50**, 27–34.
20. Tamai, N., Myoui, A., Tomita, T., Nakase, T., Tanaka, J. and Ochi, T., Novel hydroxyapatite ceramics with an interconnective porous structure exhibit superior osteoconduction in vivo. *J. Biomed. Mater. Res.*, 2002, **59**, 110–117.
21. Fabbri, M., Celotti, G. C. and Ravaglioli, A., Hydroxyapatite-based porous aggregates: physico-chemical nature, structure, texture and architecture. *Biomaterials*, 1995, **16**, 225–228.
22. Tampieri, A., Celotti, G., Sprio, S., Delcogliano, A. and Franzese, S., Porosity-graded hydroxyapatite ceramics to replace natural bone. *Biomaterials*, 2001, **22**, 1365–1370.
23. Komlev, V. S. and Barinov, S. M., Porous hydroxyapatite ceramics of bi-modal pore size distribution. *J. Mater. Sci.: Mater. Med.*, 2002, **13**, 295–299.
24. Le Huec, J. C., Schaeverbeke, T., Clement, D., Faber, J. and Le Rebeller, A., Influence of porosity on the mechanical resistance of hydroxyapatite ceramics under compressive stress. *Biomaterials*, 1995, **16**, 113–118.
25. Wang, L., Nemoto, R. and Senna, M., Microstructure and chemical states of hydroxyapatite/silk fibroin nanocomposites synthesized via a wet-mechanochemical route. *J. Nanoparticle Res.*, 2002, **4**, 535–540.
26. Izumi, F. and Ikeda, T., A Rietveld-analysis program RIETAN-98 and its applications to zeolites. *Mater. Sci. Forum.*, 2000, **321**, 198–203.